Journal of Materials Research and Technology 32 (2024) 3842–3856

Contents lists available at ScienceDirect

Journal of Materials Research and Technology

journal homepage: www.elsevier.com/locate/jmrt

Experimental review and accuracy of etchants used for phase analysis of SAF2507 Super Duplex Stainless Steel

F. Sordetti [a,*], A. Palombi [b], A. Varone [b], N. Picco [a], M. Magnan [a], E. Marin [a,c], C. Maranzana [d], A. Lanzutti [a]

[a] University of Udine, Polytechnic Department of Engineering and Architecture, Via delle Scienze 208, 33100, Udine (UD), Italy
[b] University of Rome "Tor Vergata", Department of Industrial Engineering, Via del Politecnico 1, 00133, Roma, Italy
[c] Kyoto Institute of Technology, Sakyo-ku, Matsugasaki, 606-8585, Kyoto, Japan
[d] Acciaieria Fonderia Cividale S.p.A., Via dell' Industria 40, 33043, Cividale (UD), Italy

ARTICLE INFO

Handling editor:SN Monteiro

Keywords:
Super duplex stainless steel
Solubilization annealing heat treatment
σ-phase
Etching
Murakami
XRD

ABSTRACT

The mechanical and corrosion properties of duplex stainless steels (DSS) depend on the distribution of ferrite and austenite as well as the presence of secondary phases. It is therefore necessary to accurately determine both the distribution of the phases and their morphology. The aim of this research is to define a standard method for the determination of the volume fraction of the phases present in a SAF2507 SDSS by analysing images acquired by light microscope. To do this, the material is heat-treated at 850 °C for 5 min, 15 min, 30 min, 1h, 5h to stimulate the formation of the σ-phase. The metallographic etchant capable of maximising phase contrast is then identified. Micrographic analyses are performed using different reagents at different holding times and temperatures, in order to find the best combination. A standard procedure is then defined for the image analysis. The data obtained ~~were~~ are processed to calculate the phase distribution. The results are compared with the quantitative analysis performed using X-ray diffraction as reference.

The research evidence that Kalling's reagent is best etchant for fully solubilised materials, as it accurately estimates ferrite and austenite content. On the other hand, Marble's reagent should be preferred for the detection of σ-phase. For comprehensive analysis of all phases, Murakami's reagent is recommended.

The approach defined in this paper not only improves the understanding of the microstructure of DSS, but also provides an important tool for industrial quality control and material characterisation.

1. Introduction

Duplex stainless steels (DSS) are biphasic stainless steels with a microstructure consisting of a ferrite matrix and islands of austenite, typically distributed equally to maximize mechanical properties [1–4]. The phase distribution depends on both the chemical composition of the steel and the heat treatments it has undergone [5]. Compared to ferritic stainless steels (FSS) and austenitic stainless steels (ASS), DSS are characterised by higher corrosion resistance, especially against pitting, stress, intergranular and crevice corrosion. Furthermore, due to an appropriate mix of the properties of the individual phases, DSS exhibit high mechanical properties [6]. Ferrite, the hardest phase, increases mechanical strength and corrosion resistance, while austenite leads to a significant increase in toughness and ductility [7]. This is why DSS are currently widely used in the oil-and-gas industry [8], in offshore platforms and in water desalination plants, which process fluids with high content of chloride (Cl^-), CO_2, hydrosulfuric gas (H_2S) HS^- and S^{-2} ions, at temperatures up to 80 °C that can intensify corrosive processes [9,10].

Some alloying elements such as C, Ni, N and Cu stabilise the austenitic phase, while elements such as Cr, Mo and W are considered as stabilisers of the ferritic phase [11]. The C content is typically extremely low to limit the formation of carbides, while Cr reaches particularly high values as it gives the alloy high corrosion resistance. Ni is added to increase the toughness of the material. Low N contents are able to increase mechanical strength and resistance to pitting corrosion [12]. An appropriate balance between these elements allows the two phases to be equally distributed and optimize the properties of DSS [13]. The content of the alloying elements also determines the PREN (Pitting Resistance Equivalent Number), which characterises the resistance to pitting

* Corresponding author.
E-mail address: francesco.sordetti@uniud.it (F. Sordetti).

https://doi.org/10.1016/j.jmrt.2024.08.191
Received 7 June 2024; Received in revised form 26 August 2024; Accepted 29 August 2024
Available online 2 September 2024

Table 1
Chemical composition of the SAF2507 SDSS analysed.

Co	Al	S	P	Mn	Si	Mo	Ni	Cr	Fe
0.0837	0.012	0.003	0.0353	0.524	0.963	4.032	6.85	24.82	bal.
Ca	**C**	**N**	**W**	**V**	**Ti**	**Sn**	**Pb**	**Nb**	**Cu**
0.0003	0.012	0.164	0.037	0.0632	0.0034	0.0077	0.0044	0.023	0.235

corrosion [14]. In particular, when the PREN is above 40, the material is called super duplex stainless steel (SDSS) [15] and is characterised by very high pitting resistance [16]. One of the most widely used SDSS is SAF 2507 (X2CrNiMo25-7-4, UNS32750) composed of 24–26 wt% Cr, 6–8 wt% Ni, 3–5 wt% Mo with a carbon content of less than 0.03 wt% and a nitrogen content of up to 0.35 wt% [17].

In order to guarantee the high properties of DSS, it is of paramount importance that the alloying elements remain dissolved in the material and do not precipitate as intermetallic phases, carbides and nitrides, which cause embrittlement and loss of corrosion resistance [18] due to the depletion of the matrix of alloying elements such as Cr, Mo and Ni [19]. In particular, at temperatures between 700 and 1000 °C, σ-phase, χ-phase and γ_2-phase precipitate [20,21]. Moreover, when the material is maintained between 300 and 600 °C, the phenomenon of spinodal decomposition of the ferrite phase can be observed [22] in conjunction with the precipitation of α′-phase, G-phase, R-phase, Cr nitride (Cr_2N), Cr carbide (Cr_3C_6, Cr_6C, Cr_7C_3), π-phase and ε-phase. [20,23,24]. This limits the maximum working temperature of this material to about 300 °C. The γ2-phase represents secondary austenite, produced not by cooling from the melt but by a solid state reaction, thus poorer in alloying elements and more susceptible to corrosion [18]. The χ-phase, a metastable ternary compound rich in Cr and Mo [25] with a wide range of stoichiometries, undergoes the transformation χ→σ under prolonged aging [26,27]. It is from $Fe_{36}Cr_{12}Mo_{10}$ to $Fe_{36}Cr_{12}Mo_3Ti_7$ [28]. Between the deleterious secondary phases that duplex steels can form, the σ-phase typically occurs in greater quantities, probably due to the rapid kinetics of formation and greater stability [29]. It consist of approximately 30 wt% Cr and 8 wt% Mo [30] and it has an often lamellar morphology produced by the eutectoid decomposition of ferrite according to the reaction $\delta \rightarrow \sigma + \gamma_2$. The σ-phase is a non-magnetic intermetallic compound characterised by a tetragonal crystallographic structure consisting of 32 atoms per unit cell [31]. Several studies have shown that the presence of σ-phase even in small quantities can significantly reduce the corrosion resistance and toughness of the material [32]. In particular, it was observed that when the σ-phase reaches 3 vol %, the toughness can be reduced from about 220 to 20 J at room temperature (RT) [30]. In order to reduce and remove the deleterious phases from DSS, it is necessary to perform a solubilization annealing.

A standard methodology to accurately evaluate the amount of the different phases present in the material has not yet been well defined. For example, the method proposed by ASTM E562-19e1 *Standard Test Method for Determining Volume Fraction by Systematic Manual Point Count* [33] consists of superimposing a grid on the micrograph obtained from the microscope and determining in which phase the intersection points fall. The method proved to be highly subjective and relatively slow as well as often imprecise, with errors in excess of 10% in determining the phases [34].

An interesting alternative involves the use of magnetic measurements (e.g. Fischer type Feritoscope®), exploiting eddy currents. This method is portable, fast and can be used on site, although it has a relatively limited range of applications due to the size of the probe.

A very precise technique for quantitatively measuring the phases present in a DSS is X-ray diffraction (XRD). In this technique, the penetration depth is ~50 μm and the accuracy of the results can be affected by textures [35].

The electron backscattered diffraction (EBSD technique has an extremely high resolution and enables very precise analysis [12]. The area analysed is very limited, careful sample preparation is required and the time required for analysis is often very long.

Image analysis techniques are often more accurate and faster [36].

The aim of this research is to define a standard metallographic method for the determination of the phases present in a DSS. It is known, in fact, that the mechanical and corrosion resistance properties of DSS are closely related to the distribution of the ferrite and austenite phases and in particular to the presence of secondary phases such as σ-phase, χ-phase and carbides. These microstructural constituents very negatively affect the performance of the material under all service conditions. Consequently, it is essential to conduct an accurate and precise characterisation of the phase distribution. It is crucial to have a rapid and common tool to determine these metallographic features as the light microscope analysis. In particular, after standard metallographic preparation, the etchant was selected to maximize the contrast between different phases. The scientific literature concerning the different metallographic etchant to be used to observe the microstructure of DSS is already relatively abundant [37]. Llorca-Isern et al. [38] tested Glyceregia, Groesbeck, Marble, modified Murakami, Villela, Electrochemical NaOH and Electrochemical HCl/ethanol. Vander Voort [39, 40] as well as Vander Voort and Manilova [41] also compared the use of numerous chemical and electrolyte etching, e.g. different type of Beraha's reagent and the Lichtenegger & Blöch's reagent. Kisasoz et al. [42] also used chemical etching in a glycerol solution of HNO_3, HCl and HF as well as electrochemical etching in solutions of KOH and NaOH. Varbai et al. [43] tried Carpenter's and other reagents. Michalska and Sogariska [26] used the Murakami's reagent, which allows excellent contrast between the phases, although it was shown that for relatively small ferrite contents it can be not very precise [38].

However, it is important to emphasise that the choice of reagent to correctly observe and identify all the phases present in a DSS, including the χ-phase and any nitrides and carbides, is far from simple. Most probably no etchant can satisfy all requirements. In addition, temperature and contact time with the sample surface are variables that greatly influence the final result.

In this research, a standard procedure was defined for the etching of the DSS and the subsequent image analysis, which was performed with image processing software in a way that was repeatable for all analysed samples. The data obtained were processed to quantitatively determine the phase distribution. The results were compared with qualitative phase analysis by XRD.

This approach represents a major step forward in the knowledge of the material. In particular, it makes it possible to select the most appropriate reagents according to the type of analysis to be performed. The wide choice of etchants and numerous experimental conditions have made it possible to achieve a remarkably detailed knowledge of metallographic techniques to be used with this class of materials.

2. Materials and methods

2.1. Analysed material

The material analysed was extracted from a solubilised cast of SAF2507 SDSS, whose chemical composition is shown in Table 1. The material was cut into 20 × 20 × 10 mm samples with a refrigerated grinding wheel. The extracted samples were heat-treated in a *Nabertherm N11/HR* laboratory furnace at 850 °C for holding times of 5 min, 15 min, 30 min, 1h, 5h and then quenched in water. The aim of this heat treatment is to stimulate σ-phase precipitation. The temperature and

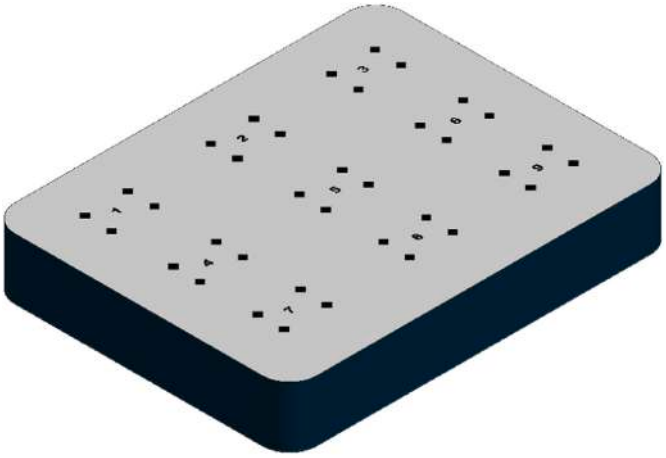

Fig. 1. Schematic representation of the 9 analysed areas for each analysed sample.

Table 2
List of used reagents and etching conditions.

Reagent	Composition	Etching conditions
Beraha	20 ml HCl 80 ml H_2O 1g $K_2S_2O_5$	few seconds of immersion at room temperature
Carpenter	15 ml HCl 85 ml ethanol	15 min, 30 min, 45 min and 60 min of immersion at room temperature
Groesbeck	4g $KMnO_4$ 4g NaOH 100 ml H_2O	10 min of immersion at 80 °C
Kalling No.2 (waterless Kalling)	5g $CuCl_2$ 100 ml HCl 100 ml ethanol	few seconds of immersion at room temperature
Lichtenegger & Blöch LB1	20g NH_4FHF 0.5 g $K_2S_2O_5$ 100 ml hot H_2O	5 min of immersion at 35 °C
Marble	4g $CuSO_4$ 20 ml HCl 20 ml H_2O	from a few seconds to a few min of immersion time at room temperature
Murakami	10g NaOH or KOH 10g $K_3Fe(CN)_6$ 100 ml H_2O	5 min, 15 min and 30 min of immersion at 80 °C
Vilella	1g picric acid 5 ml HCl 100 ml ethanol	1 min, 5 min, 15 min and 30 min of immersion at room temperature

holding times of the ageing heat treatment were chosen in accordance with the scientific literature [11]. The temperature and the holding times were chosen in accordance with the typical cooling transformation curves of this material [44] in order to achieve increasing σ-phase contents.

2.2. XRD analysis

XRD analysis was used to obtain quantitative results of the phase distribution. In particular, XRD patterns have been recorded in the 2θ angular range 15–55° by using the Mo-Kα radiation (λ = 0.0709 nm). XRD spectra were collected in step-scanning mode with 2θ angular steps of 0.05° and counting time per step of 4 s. The phases have been identified and the corresponding reflections indexed according to the JCPDS database [45].

To determine the fractions of ferrite, austenite and σ-phase present in DSS in its original condition and after heat treatments, XRD precision peak profiles have been collected with 2θ angular steps of 0.005° and counting time per step of 4 s. The method to calculate the relative amount of each phase is described in Appendix A. The obtained results are discussed and compared to the scientific literature available on this topic. The values obtained for α, γ and σ phases are considered as reference for this work.

2.3. Microstructural characterization

The calculated phase distribution was compared with the quantitative results obtained from the XRD analysis, taken as a reference. The phase analysis was performed by observing the etched samples, that underwent a preliminary metallographic preparation, under a *Zeiss Axio Vert. A1* optical microscope equipped with a *Zeiss Axiocam 208 Color* digital camera at 100× magnification.

On each sample, as illustrated in Figs. 1 and 9 different zones were identified through microhardness indentation. In these zones, optical micrographs were acquired and used to determine the quantity of the different phases through image analysis techniques. The same 9 zones were used for all the different metallographic etchants investigated. To determine the accuracy of the experimental data obtained from the phase analysis, the same procedure was repeated by first analysing a single image, then averaging the results of 3, 6 and all the 9 images.

2.4. Etchant selection

The etchants, listed in Table 2, were selected according to the specific scientific literature, as described in the Introduction section. In particular:

- Beraha's reagent [39,40] colours ferrite and provides high phase contrast. It is a widely used reagent for image analysis. It requires the sample to be kept immersed at room temperature until the surface is coloured. It is recommended to store the solution for at least 24 h before use. The sample is then rinsed in acidic solution;
- Carpenter's reagent [43] reveals ferrite, phase boundaries and σ-phase. It requires immersing the sample in the reagent for 15–45 min at room temperature;
- Groesbeck's reagent [38] colours the carbides black, the σ-phase dark grey and does not attack either ferrite or austenite. It requires immersing the sample for about 10 min in the reagent heated from 60 °C to 90 °C. The sample is rinsed in acidic solution and then in ethanol;
- Kalling's No.2 reagent [43] etches ferrite quickly and austenite very slowly. No secondary phases can be observed. Etching requires immersion or swabbing for a short time at room temperature;
- Lichtenegger & Blöch's LB1 reagent [40,41] colours austenite and quickly attacks the secondary phases. It is necessary to immerse the sample for several min in the reagent heated at about 30 °C;
- Marble's reagent [38] etches the σ-phase. It requires immersion or swab for 5–60 s at room temperature;
- Murakami's reagent [26,38] colours the ferrite orange, the σ-phase very dark blue and the carbides black. Etching requires immersing the sample in the heated reagent at about 80 °C for up to 60 min;
- Vilella's reagent [38] highlights the deleterious phases. The etching requires immersion from a few seconds to several min in the reagent at room temperature.

2.5. Image analysis

The images obtained were processed with the image analysis software *ImageJ* (ImageJ 1.53a, Wayne Rasband, National Institutes of Health, USA). The procedure used, shown schematically in Fig. 2, consist of:

- a preliminary image cropping, to remove the part containing the hardness indentations and the measurement marker, in order not to consider them in the phase count;
- a greyscale image conversion;

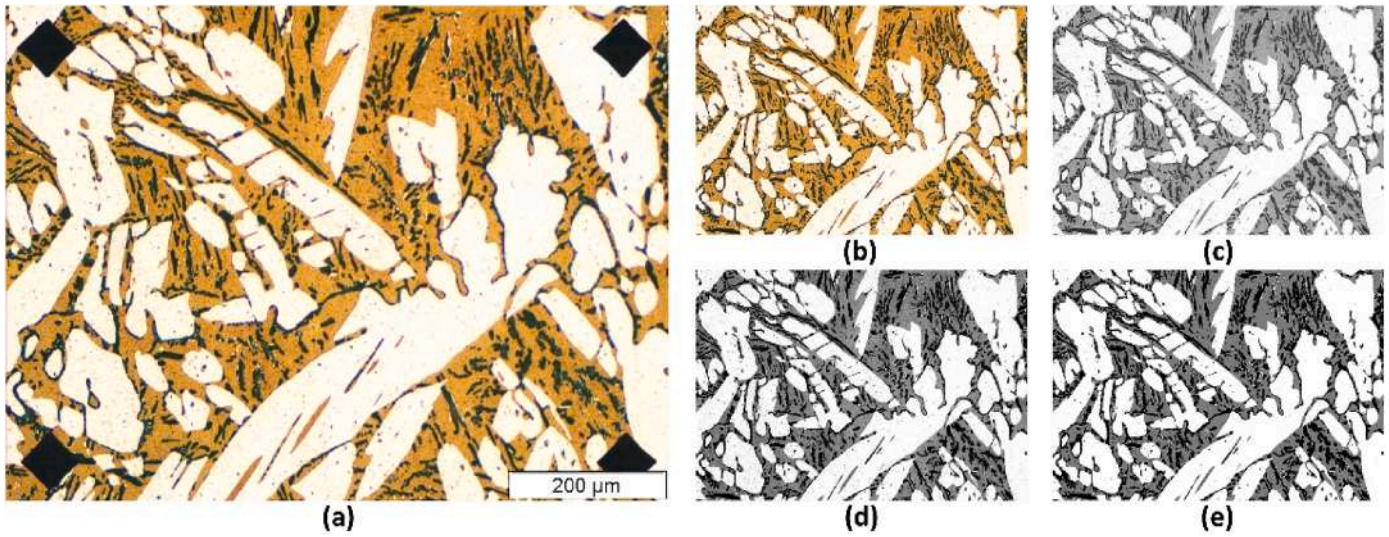

Fig. 2. Image analysis procedure: (a) original image, (b) image cropping, (c) greyscale conversion, (d) contrast adjustment, (e) three tones binarization.

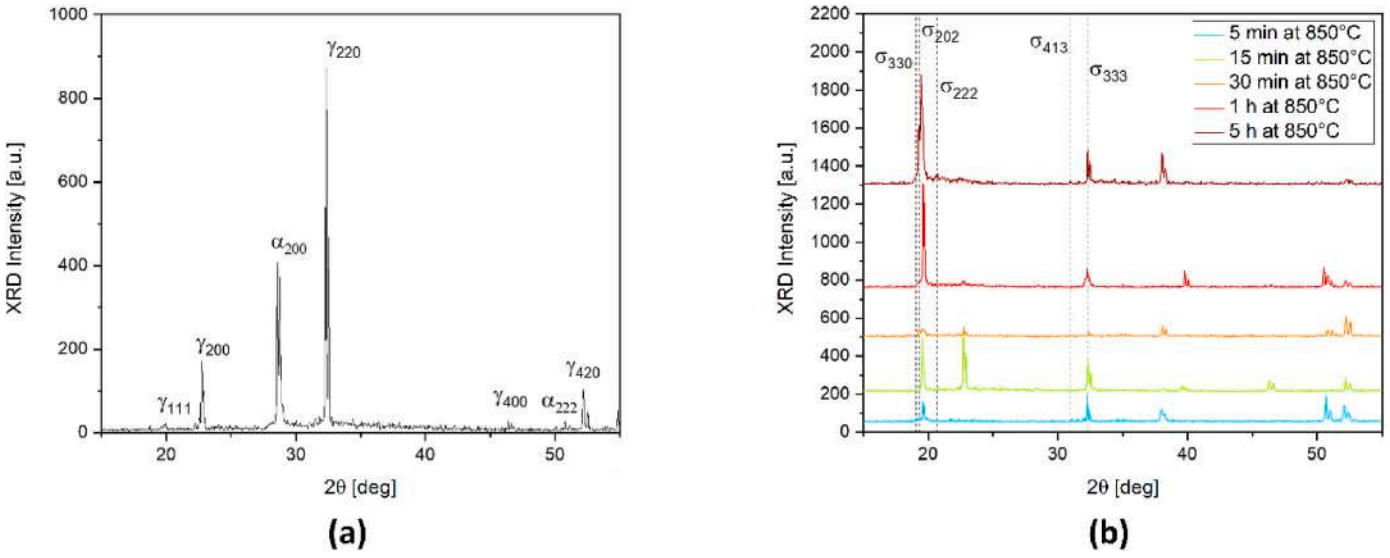

Fig. 3. XRD pattern of all samples analysed: (a) solubilised, (b) heat treated at 850 °C.

- an automatic contrast adjustment, in order to obtain the same average contrast value in all analysed images;
- an image binarization, to obtain a number of tones equal to the number of phases present in the material: two tones, if only ferrite and austenite are present, or three tones, if the σ-phase is also present. In the first case, the process uses the greyscale intensity histogram and applies an automatic threshold calculated as half of the maxima of the peaks, thus corresponding to the maximum contrast. All pixels lighter than this threshold were coloured white and all darker pixels black. A similar process was applied to the samples with three phases.

The same result can be achieved with software such as *Gimp* or *Adobe Photoshop*.

The phase distribution was calculated by extracting histogram data that quantifies the number of pixels corresponding to each tonal value present in the image. By importing the histogram data into a calculation software such as *Microsoft Excel*, it was finally possible to obtain the percentage of each phase present by calculating the ratio between the pixels corresponding to each of them. This procedure is in agreement to ASTM E562-19e1 *Standard Test Method for Determining Volume Fraction by Systematic Manual Point Count* [46] that suggests the use of grids for the evaluation of phase content. In this case the grid is composed by a matrix of vertical and horizontal pixels that corresponds to image resolution.

3. Results and discussion

3.1. XRD analysis

The samples investigated were analysed by XRD in fully solubilised condition and after heat treatment at 850 °C with holding times of 5 min, 15 min, 30 min, 1 h and 5 h. The graphs of Fig. 3 show the overlay of the complete XRD spectra used to identify the phases.

As expected, the untreated material consists only of ferrite and austenite (Fig. 3(a)) while the σ-phase has been detected in all heat treated samples. Comparing the spectra (Fig. 3(b)), it is possible to observe that the relative intensities change with heat treatment holding time indicating a variation in the amount of each phase. In particular, the σ-phase forms at expenses of ferrite and its relative amount increases

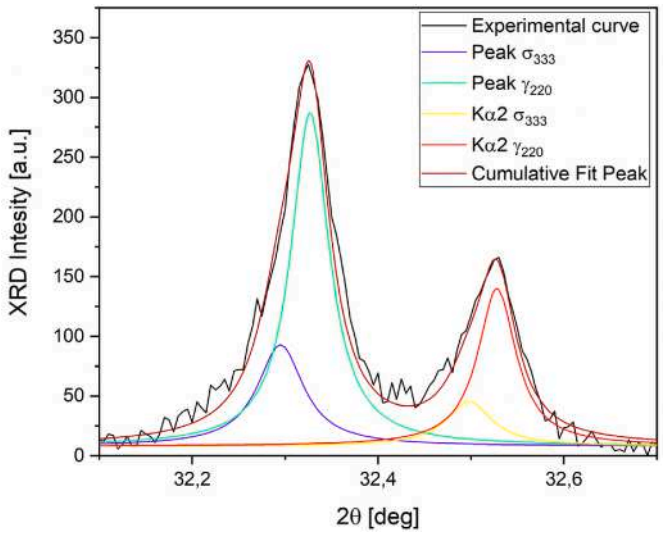

Fig. 4. Precision peak in the 2θ range of 32,0–32.8° of sample heat treated for 15 min at 850 °C.

with heat treatment time [20,21,23,24].

Quantitative analysis was performed from high precision XRD measurements of each peak, fitting the experimental curves to determine the peak parameters. An example is reported in Fig. 4, the experimental curve can be fitted with 4 Lorentz peaks (two main peaks and the two corresponding Kα2 peaks).

All fittings were performed by considering the following conditions: (i) the full width at half maximum (FWHM) of Kα1is equal to the FWHM of Kα2, (ii) the intensity of the Kα1 peak is two times the intensity of Kα2 peak.

The same procedure has been applied to every peak, to determine the integrated peak intensity, used to calculate the amounts of each phase by the method explained in Appendix A. The results are shown in Fig. 5 (dots), where the continuous curves were obtained as a logarithmic interpolation of the experimental data, in accordance with the kinetics of phase evolution in this material [47].

3.2. Etchant selection

The metallographic etchings obtained using Beraha's reagent, as illustrated by the micrographs in Fig. 6, are characterised by a very high contrast. It is important to highlight, that this reagent does not attack the σ-phase, which is therefore indistinguishable from the ferritic phase. For this reason, Beraha's reagent can only be used to determine the phase distribution on completely solubilised samples. It should be noted that the reagent also has a tendency to stain the austenitic phase, making image analysis more difficult.

During immersion of the sample in the solution, nothing happens for several seconds. Afterwards, the film of passivity breaks down and the surface darkens rapidly. It is necessary to extract and rinse the sample quickly to avoid excessive etching. Otherwise, a deposit may form on the surface, which also darkens the austenite. In this case, a light polish of surface is required to obtain a high quality image.

Another etchant selected for this experience is the Carpenter's reagent. In order to optimize the image quality of the etched surface, the immersion time of 15 min, 30 min, 45 min and 60 min was used. A selection of the micrographs obtained is shown in Fig. 7. With a short immersion time the etchant produces sufficient contrast between ferrite and austenite in a fully solubilised sample and it does not stain the surface. In samples with the presence of σ-phase, as shown in Fig. 7(b1) and Fig. 7(b2), Carpenter's reagent reveals all the phases (ferrite, austenite and σ-phase), but the contrast is very low. For longer immersion time the etchant highlights better the phases, but causes a dark halo around the σ-phase that makes its quantification difficult. Increasing the immersion time, it worsens the resolution already at low amounts of sigma phase. In the fully solubilised samples (Fig. 7(a2) and Fig. 7(a3)), only the boundaries of the different phases are highlighted, without any contrast between them. In conclusion, phase determination with this reagent is difficult and imprecise.

Another etchant suggested by literature to highlight the phases in DSS in the Groesbeck's reagent that darkens the σ-phase, as shown in the images of Fig. 8. For this reason, this reagent is very useful to distinguish the σ-phase even at very low amounts. On the other hand, the austenite and the ferrite are not clearly resolved.

The Kalling's No.2 reagent, shown in Fig. 9, etches intensively the ferrite phase. However, in the fully solubilised sample, as shown in Fig. 9

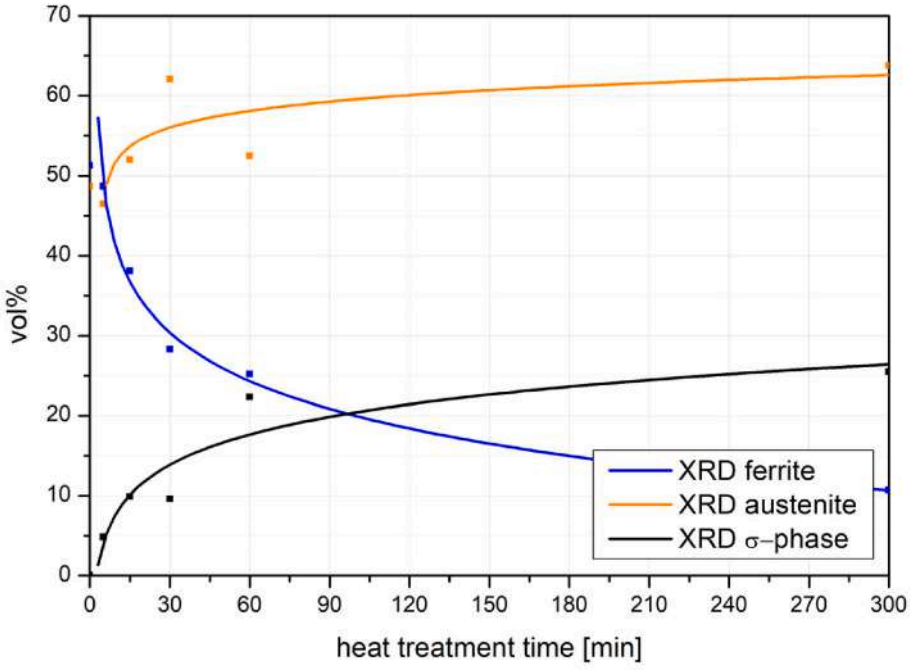

Fig. 5. Volumetric phase distribution of all samples analysed with XRD.

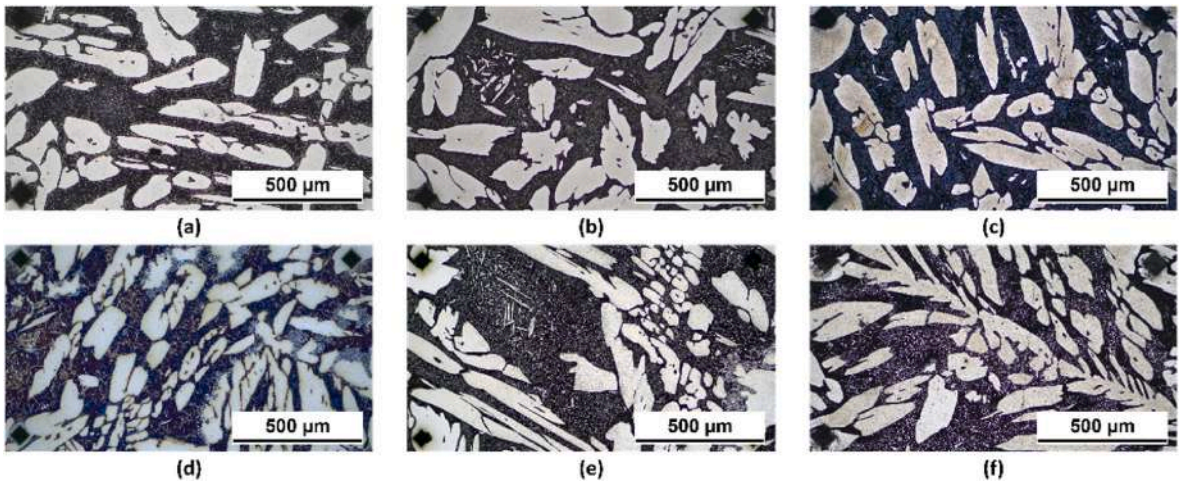

Fig. 6. Beraha's reagent: (a) solubilised, (b) 5 min at 850 °C, (c) 15 min at 850 °C, (d) 30 min at 850 °C, (e) 1 h at 850 °C, (f) 5 h at 850 °C.

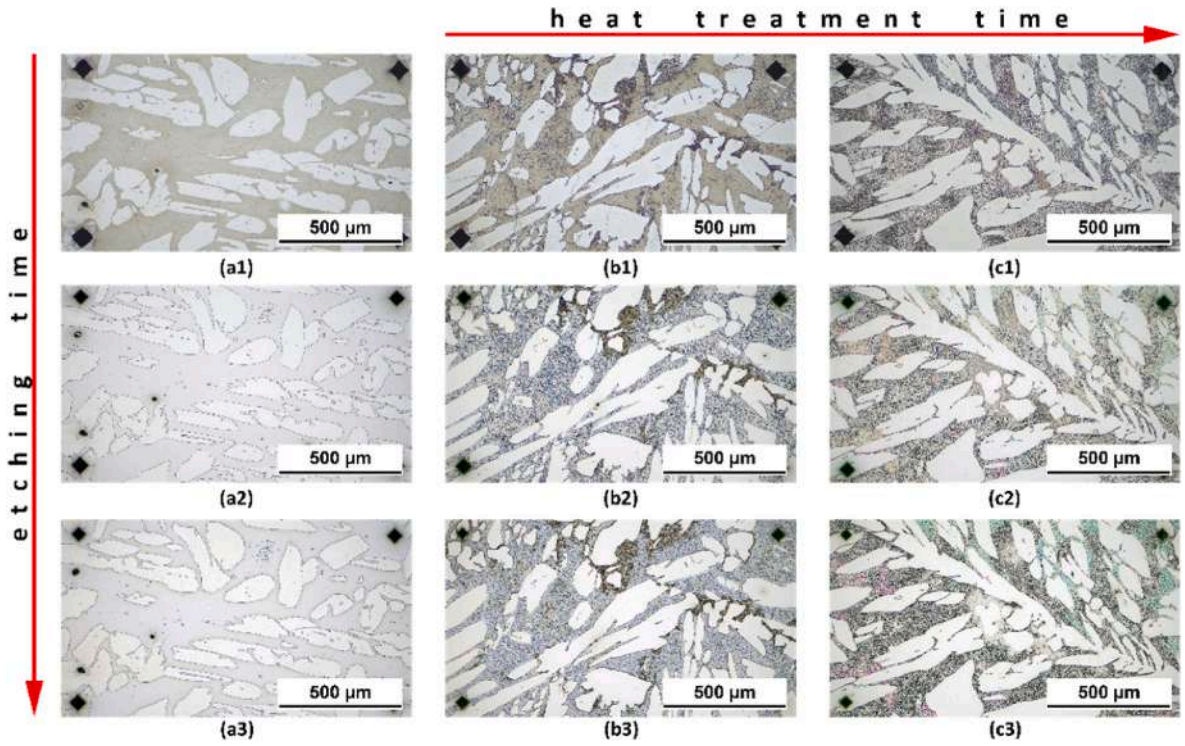

Fig. 7. Carpenter's reagent: (a-) solubilised, (b-) 30 min at 850 °C, (c-) 5 h at 850 °C, (−1) 15 min of immersion, (−2) 30 min of immersion, (−3) 60 min of immersion.

(a), the etching is very light, even after a long immersion time, mainly because of the robust passivity film of a σ-phase-free SDSS. In samples with σ-phase, ferrite colours quite homogeneously and the σ-phase is not easily resolved. In general, the contrast is not sufficient to perform an accurate image analysis to distinguish the σ-phase.

Etching the samples with Lichtenegger & Blöch's LB1 reagent requires immersion for about 5 min at 35 °C, until the surface darkens. As illustrated in the selection of micrographs in Fig. 10, in samples with little or no σ-phase, the austenite darkens. This is not the case in samples with more content of this deleterious phase, in which the distinction between ferrite and austenite becomes very difficult due to the low contrast. When verifying the presence of σ-phase, the best practice is to etch the sample for a long time (several minutes) until the σ-phase darkens, and then polish the surface with the last cloth used in the metallographic preparation.

The Marble's reagent, as shown in Fig. 11, effectively darkens the σ-phase in few tens of seconds of immersion time, when its amount is very high. When its content is low, etching time have to be prolonged to tens of minutes, until the film of passivity breaks down. As already described for other etchants, if the sample is immersed for too long time, the austenitic phase also starts to darken. After the etching, it is sufficient to light polish the sample to remove the patina and obtain a very good contrast between the σ-phase and the other phases.

The most widely used etchant for microstructural characterization of SDSS is the Murakami's reagent. In particular, by immersing the fully solubilised samples in the etchant for 5 min, as shown in the micrographs in Fig. 12(a1), the contrast between ferrite and austenite is always quite low. When a small amount of σ-phase is present, as in the micrograph in Fig. 12(b1), the contrast between the σ-phase and the other phases is good. When there is a large amount of σ-phase, as

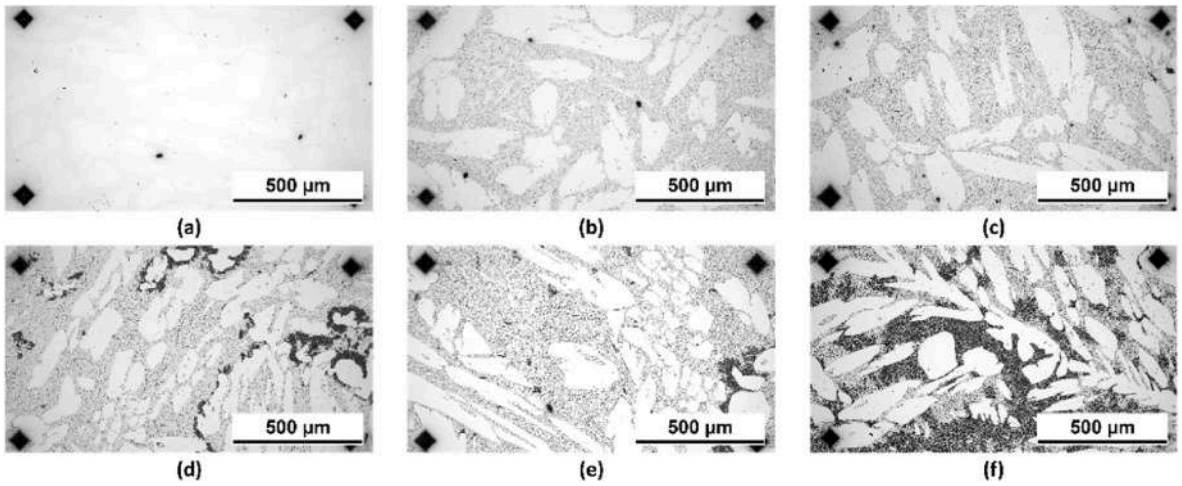

Fig. 8. Groesbeck's reagent: (a) solubilised, (b) 5 min at 850 °C, (c) 15 min at 850 °C, (d) 30 min at 850 °C, (e) 1 h at 850 °C, (f) 5 h at 850 °C.

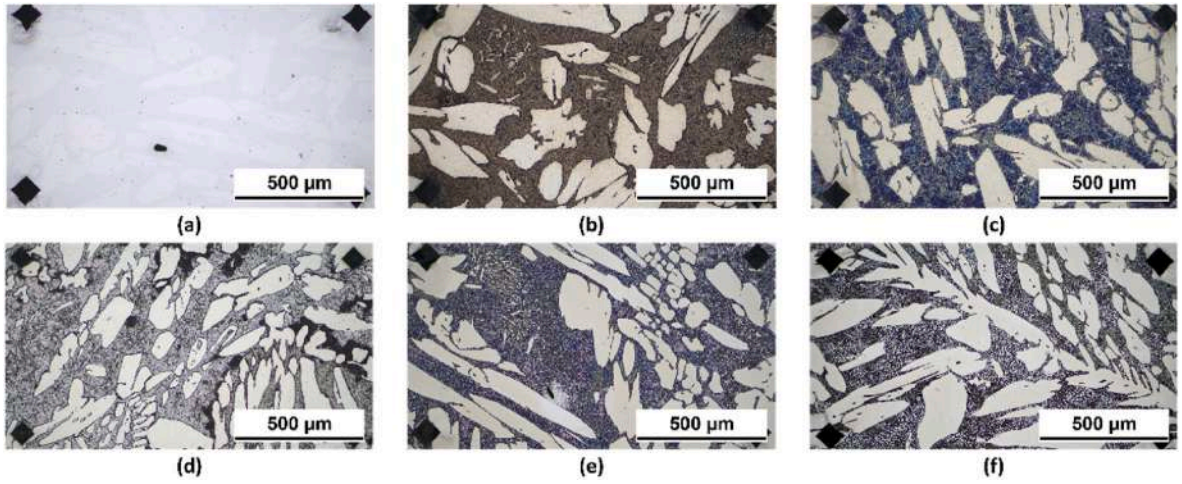

Fig. 9. Kalling's No.2 reagent: (a) solubilised, (b) 5 min at 850 °C, (c) 15 min at 850 °C, (d) 30 min at 850 °C, (e) 1 h at 850 °C, (f) 5 h at 850 °C.

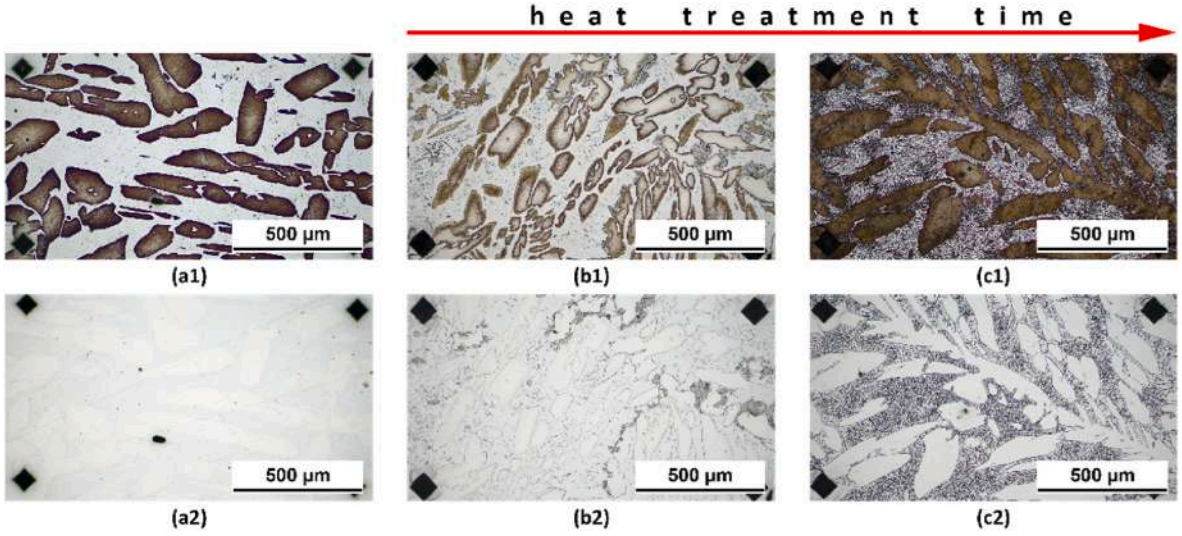

Fig. 10. Lichtenegger & Blöch's LB1 reagent: (a-) solubilised, (b-) 30 min at 850 °C, (f-) 5 h at 850 °C, (−1) etched, (−2) etched and polished.

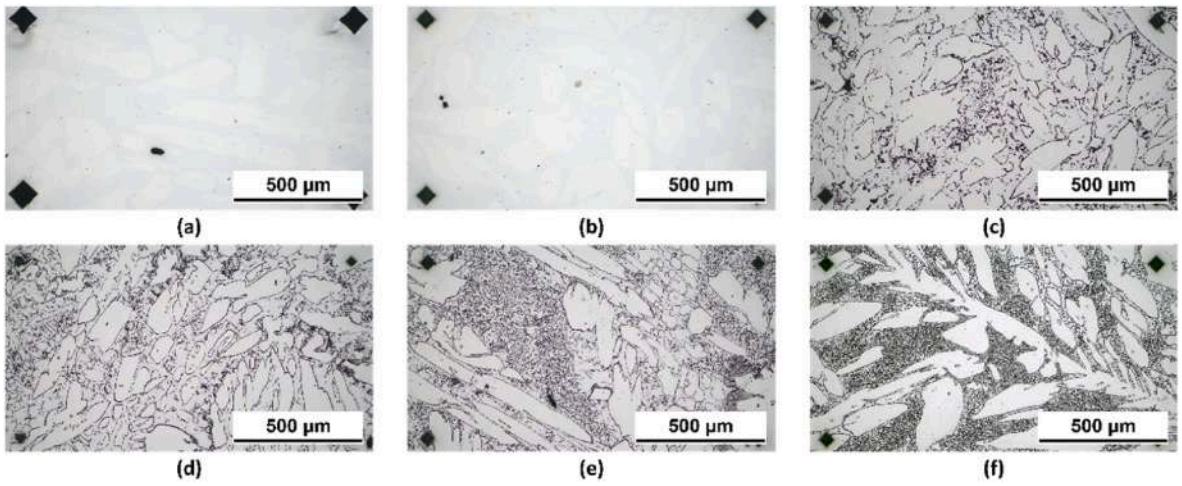

Fig. 11. Marble's reagent: (a) solubilised, (b) 5 min at 850 °C, (c) 15 min at 850 °C, (d) 30 min at 850 °C, (e) 1 h at 850 °C, (f) 5 h at 850 °C.

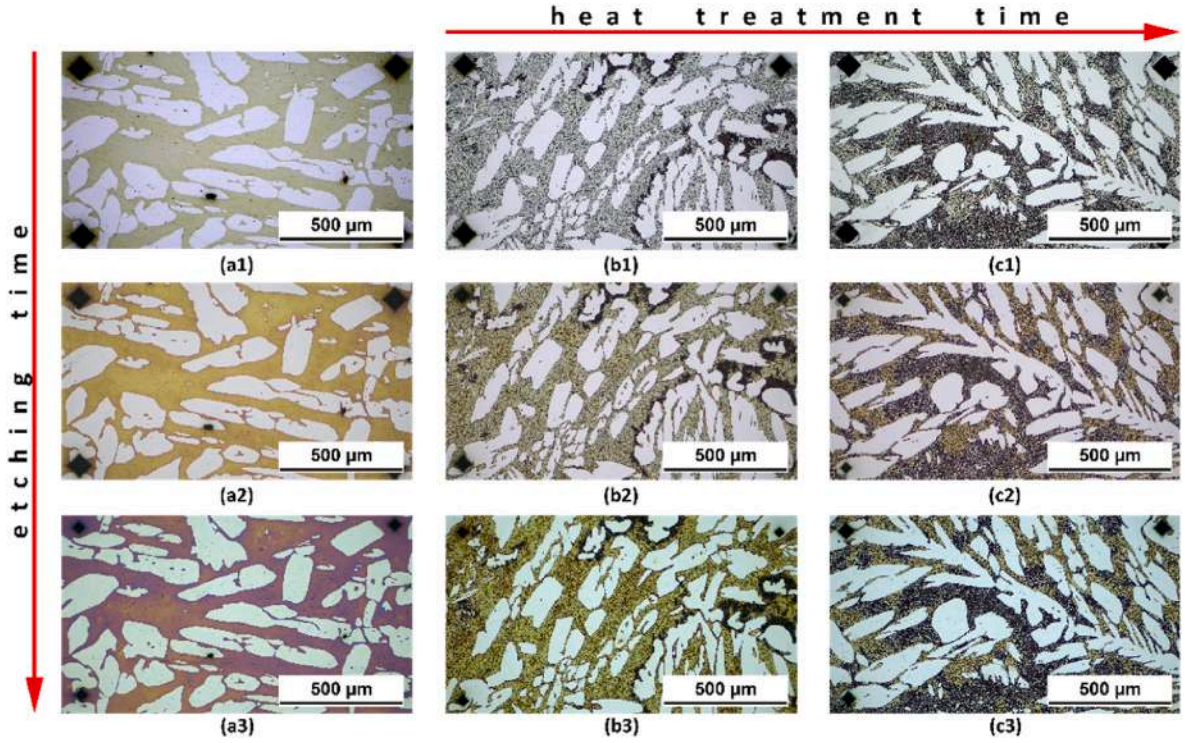

Fig. 12. Murakami's reagent: (a-) solubilised, (b-) 30 min at 850 °C, (c-) 5 h at 850 °C, (−1) 5 min of immersion, (−2) 15 min of immersion, (−3) 30 min of immersion.

illustrated in Fig. 12(c1), the σ-phase is faded and the other phases present are very difficult to distinguish.

By increasing the etching time to 15 min (Fig. 12(a2), Fig. 12(b2) and Fig. 12(c2)), a better contrast between the phases is observed. In the fully solubilised samples and those with a low σ-phase content, it is possible to identify all phases with good accuracy. On the other hand, in the samples with a high σ-phase content, the immersion time is probably still too short to obtain a good contrast.

Extending the immersion time to 30 min in Murakami's reagent, an excellent contrast between all the phases is obtained for all the tested samples. However, when the samples are fully solubilised, as shown in Fig. 12(a3) the ferrite takes a dark orange colour. This suggests that etching times longer than 30 min should be avoided due to the loss of contrast.

The last reagent is the Vilella's, widely used to etch martensitic stainless steels. In the micrographs of the samples etched with this reagent, shown in Fig. 13, it can be observed that immersion times shorter than 15 min highlight only the σ-phase with a good contrast.

For longer immersion times, as illustrated in the images from Fig. 13 (a4) to Fig. 13(c4), the ferrite starts to darken heavily, which makes image analysis in most cases rather complex. Only in the case of the fully solubilised material it is possible to obtain a good contrast between ferrite and austenite.

3.3. Image analysis

3.3.1. Ferrite and austenite detection

The image analysis performed on the samples etched with Beraha's

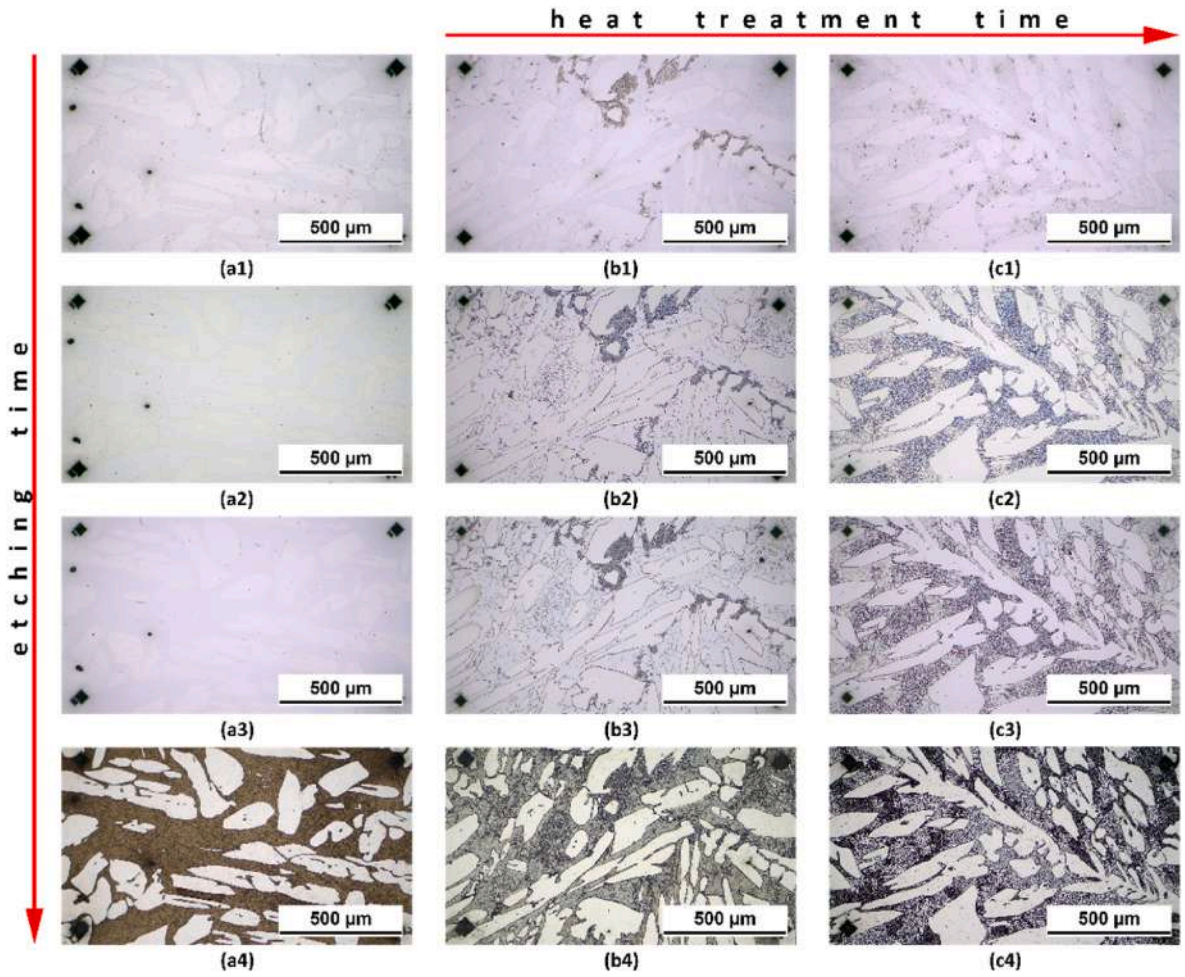

Fig. 13. Vilella's reagent: (a-) solubilised, (b-) 30 min at 850 °C, (c-) 5 h at 850 °C, (−1) 1 min of immersion, (−2) 5 min of immersion, (−3) 15 min of immersion, (−4) 30 min of immersion.

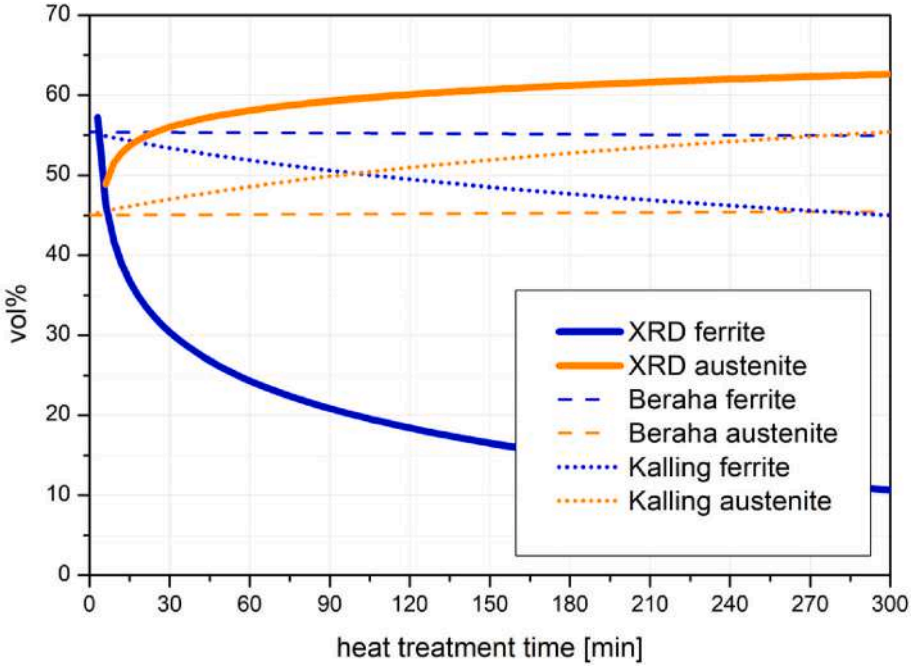

Fig. 14. Comparison of volumetric phase distribution of samples heat treated at 850 °C: XRD and image analysis results of samples etched with Beraha's and Kalling's reagents.

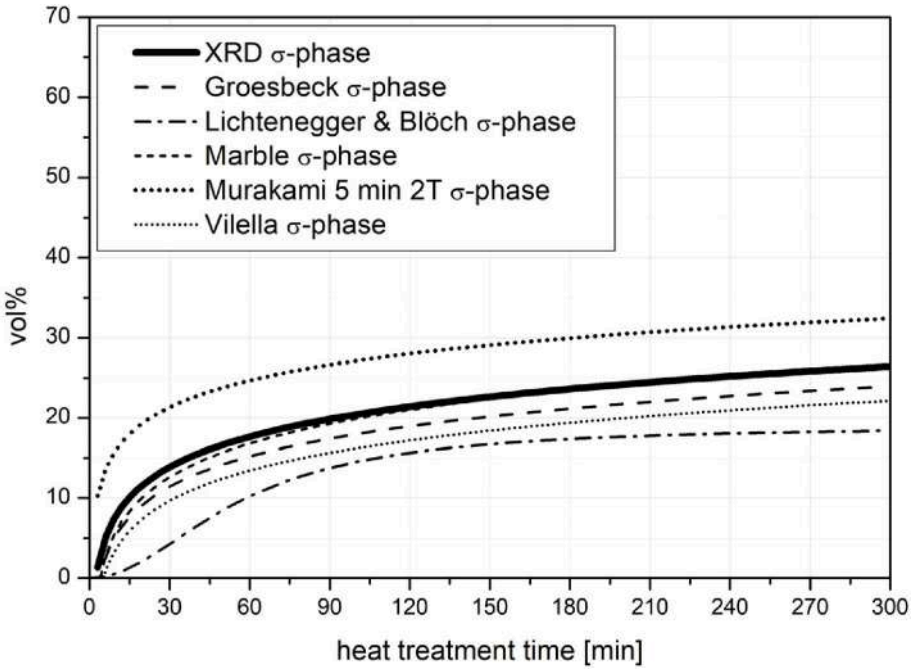

Fig. 15. Comparison of volumetric phase distribution of samples heat treated at 850 °C: XRD and image analysis results of samples etched with Vilella's (5 min of immersion time), Marble's, Murakami's (5 min of immersion time, 2 tones image analysis), Groesbeck's and Lichtenegger & Blöch's reagents.

reagent makes it possible to distinguish only the unetched austenitic phase from the rest of the microstructure. In fact, both the σ-phase and the ferrite are coloured black. The high contrast makes the analysis easy and accurate. As reported in the diagram in Fig. 14, the image analysis shows that as the heat treatment time varies, the quantity of the analysed phases remains constant. In particular, ferrite has a content of about 55% by volume and austenite about 45%.

Even from the image analysis of the samples etched with Kalling's No.2 reagent, it was only possible to evaluate the amount of ferrite and austenite present in the samples examined. As can be seen from the diagram in Fig. 14, the trend of the two phases is inverse. In particular, the amount of ferrite decreases as the heat treatment time increases, while that of austenite increases with the same law.

The constant trend obtained from the Beraha's reagent may be due to the fact that the σ-phase is produced within the ferritic phase, and, at least for sufficiently short treatment times, the quantity of austenite should remain constant. On the other hand, the result obtained from the Kalling's reagent is in agreement to XRD data. In fact, the 55-45% distribution between ferrite and austenite is typical of the solubilization annealing heat treatment at approximately 1100 °C that the material analysed has undergone. During the heat treatment at 850 °C performed to stimulate the formation of the σ-phase, for long times the balance between ferrite and austenite also shifts towards this last phase. This justifies the trend shown in the graph.

Analysing the results, it can be concluded that the most reliable trend is obtained from the image analysis performed on the samples etched with Kalling's reagent.

3.3.2. σ-phase detection

The image analysis of the samples etched with Groesbeck's reagent, the results of which are reported in the diagram in Fig. 15, show an increasing trend of the σ-phase with heat treatment time with a logarithmic law, in agreement to the kinetics of formation of this deleterious phase. The high contrast generated by this type of etching allows for very precise and accurate image analysis.

In samples etched with the Lichtenegger & Blöch's LB1 reagent, the increase of then σ-phase over time appears very slow up to 15 min and then increases more quickly up to 60 min, beyond which the increase becomes more moderate again. Also in this case, the high contrast generated by the reagent allows rapid and accurate image analysis.

As already described for other types of reagents, even in samples etched with Marble's reagent, after a short polishing time the contrast between the σ-phase and the rest of the phases is very high and allows a good image analysis. Again, the increase in σ-phase is logarithmic with time [47].

From the image analysis of the samples etched with Vilella's reagent for an immersion time of 5 min, considered the best for this type of analysis, is evident that even in this case the time increasing of the σ-phase has a logarithmic law, in accordance with the precipitation kinetics of this deleterious phase in the material. The analysis is very simple and accurate due to the high contrast present in the micrographs.

The comparison of the results of the image analysis highlight that Marble's, Grossbeck's and Vilella's reagents produce essentially comparable image analysis results. The 2-tone image analysis performed on samples etched with Murakami's reagent for 5 min of immersion time overestimates the σ-phase content, probably due to excessive darkening of the ferrite. On the other hand, in the samples etched with Lichtenegger & Blöch's reagents the σ-phase is underestimated, probably due to the poorly contrasted etching. It can be concluded that the etching that best approximates the XRD results is Marble's reagent. Very similar results are also obtained with the Groesbeck reagent.

3.3.3. All phases detection

The result of the image analysis of the samples etched with Murakami's reagent for different immersion times is shown in the diagram in Fig. 16.

Concerning the ferritic phase, in samples etched for a short time, the low contrast slightly underestimates the ferrite which is very light and can be confused with the austenite. In samples immersed for a long time, probably due to excessive darkening of this phase, the ferrite is underestimated as it is confused with the σ-phase. Samples immersed for 15 min produce a higher content of this phase.

From a comparison between the three different immersion times, the most homogeneous results appear to be those relating to the 15 min etching.

The austenite has a constant trend with different heat treatment

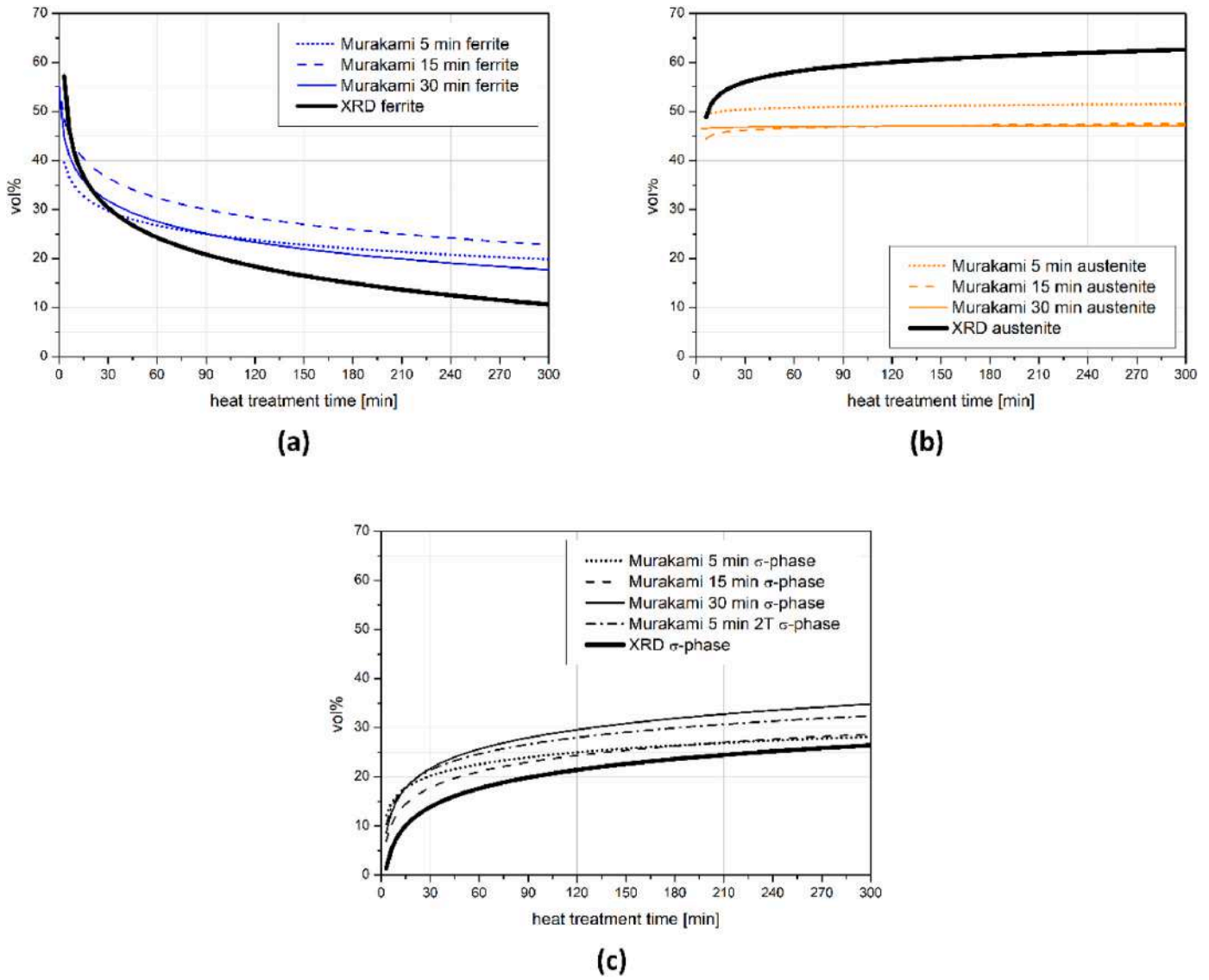

Fig. 16. Comparison of volumetric phase distribution of samples heat treated at 850°: XRD and image analysis results of samples etched with Murakami's reagent (a) ferrite, (b) austenite, (c) σ-phase.

time, as the σ-phase is known to precipitate within the ferritic phase. The etchings performed with immersion times of 15 and 30 min, due to the good contrast between the unetched austenite and the rest of the microstructure, allow equal image analysis results of approximately 47% austenite. In the samples etched with a shorter immersion time, on the other hand, the austenite is slightly higher, probably due to the low contrast that confuses other clear parts of the micrograph with this phase.

As regards the σ-phase, in samples etched for immersion times lower than 30 min, probably again due to the low contrast, the image analysis produces slightly lower results compared to samples immersed for 30 min.

The comparison of the phase distribution obtained with the XRD technique and the image analysis performed on the micrographs of the samples etched with Murakami's reagent for different immersion times shows that this reagent overestimates both the ferrite and the σ-phase, while the austenitic phase is underestimated. This difference is probably due to the fact that Murakami's reagent is a colouring reagent that probably makes a stain on the surface of the analysed samples. Where the stains are dark, they are calculated by the image analysis as σ-phase while where the stains are lighter, they are probably mistaken with ferrite. Another source of image analysis error that causes the underestimation of the austenitic phase is probably due to the presence of a certain amount of secondary austenite, typically very small and uniformly distributed within the ferritic phase. As is known [20], this phase forms as a consequence of the formation of the σ-phase, which locally depletes the ferrite of strongly ferritising elements such as Cr and Mo. This chemical unbalance results in the formation of secondary austenite. The relatively low resolution of optical microscopy combined with the possibility of staining of the etching may explain the underestimation of the austenitic phase.

3.3.4. *Accuracy of experimental data*

Fig. 17 shows the comparison between the results obtained from the image analysis of the samples in which Kalling's reagent, considered the best for analysing the ferritic and austenitic phases, was used.

As can be seen, the trend lines obtained by interpolating the results of the analysis of 3, 6 and 9 images with a logarithmic law are very similar to each other. On the other hand, the result obtained from analysing a single image significantly differs and generates a larger dispersion of the data. Furthermore, when analysing a single image, choosing different areas of the sample surface produces different results. For these reasons,

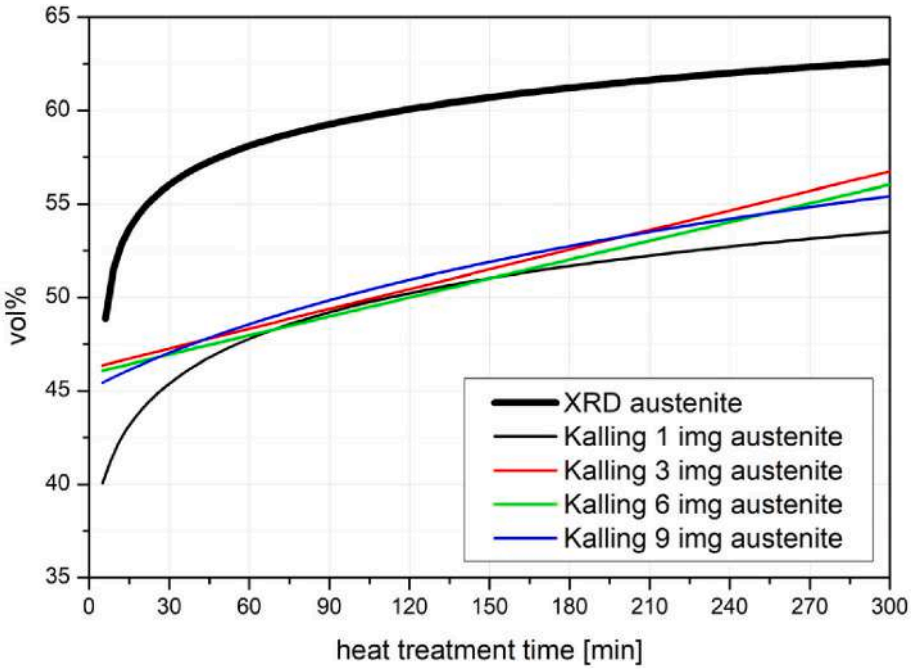

Fig. 17. Comparison of volumetric phase distribution of samples heat treated at 850 °C, XRD and image analysis with 1, 3, 6 and 9 micrographs of samples etched with Kalling's reagent: austenite trend lines.

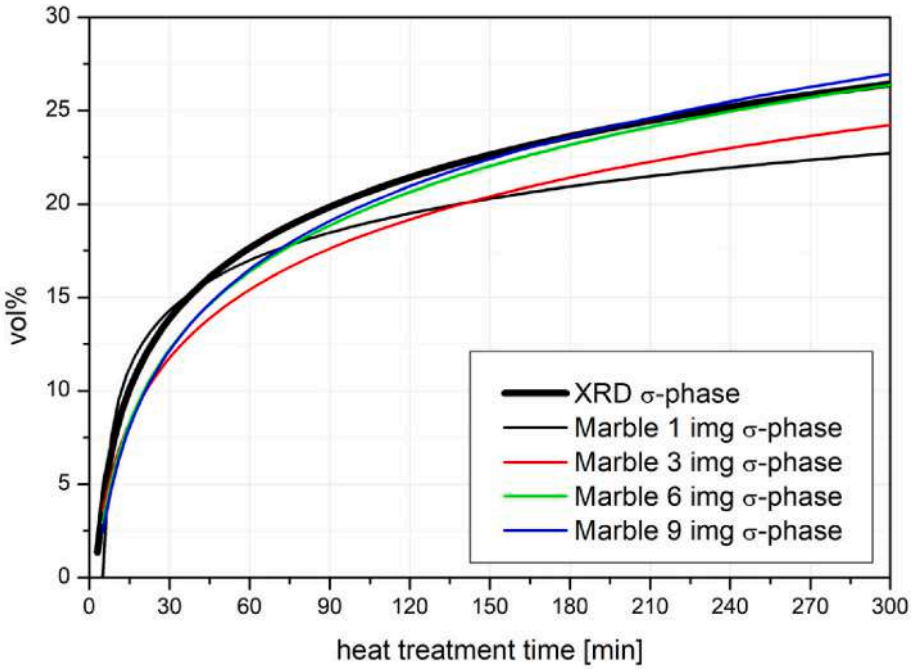

Fig. 18. Comparison of volumetric phase distribution of samples heat treated at 850 °C, XRD and image analysis with 1, 3, 6 and 9 micrographs of samples etched with Marble's reagent: σ-phase trend lines.

it is always recommended to perform an image analysis on a minimum number of 3 micrographs.

The results of the image analysis performed on the samples etched with Marble's reagent, the best choice for visualising only the σ-phase, are shown in Fig. 18. In this case, observing the trend lines, it can be concluded that at least 6 images are required to obtain repeatable results.

As for the samples etched with Murakami's reagent, the results of the image analysis shown in Fig. 19 indicate that the trend lines are very similar when analysing a minimum of 3 micrographs.

4. Conclusions

In this research, we proposed a new standardized method for estimating the volume fraction of the phases in a SAF2507 SDSS. The material, initially in the solubilised state, was subjected to a heat treatment at 850 °C for several holding times in order to stimulate σ-phase precipitation. Numerous etchants were compared and their use optimised to

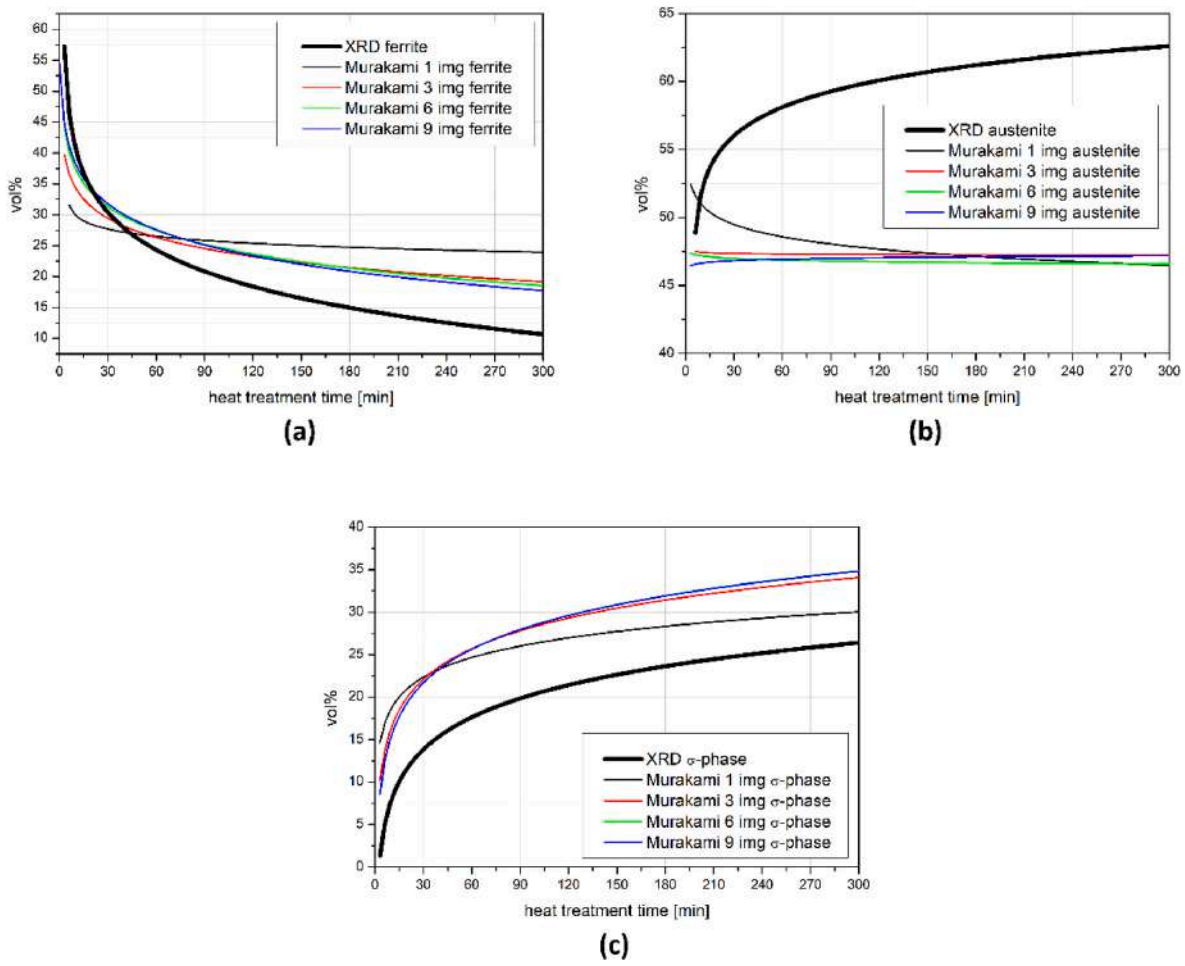

Fig. 19. Comparison of volumetric phase distribution of samples heat treated at 850 °C, XRD and image analysis with 1, 3, 6 and 9 micrographs of samples etched with Murakami's reagent: (a) ferrite trend lines, (b) austenite trend lines, (c) σ-phase trend lines.

maximize the contrast between ferrite, austenite and secondary phases. A standard and reliable procedure for calculating the phase distribution was established.

From the results of the image analysis, it can be concluded that:

- the easiest etchant to determine the phases in fully solubilised condition is Beraha's reagent, used for a few seconds of immersion at room temperature;
- the Marble's reagent (a few seconds to a few min of immersion at room temperature), Groesbeck's reagent (10 min of immersion at 80 °C) and Lichtenegger & Blöch's reagent after polishing (5 min of immersion at 30 °C) are the most suitable etchants to detect the σ-phase;
- the Murakami's reagent, with an immersion time of at least 15 min and no more than 30 min, is the best etchant to highlight all the phases in a single etching.

Comparing the XRD results, used as a reference, with the image analysis, the most accurate results were obtained with:

- the Kalling's reagent for the evaluation of the ferrite and austenite content in fully solubilised condition;
- the Marble's reagent to detect and quantify only the σ-phase at room temperature operations. On the other hand, the Groesbeck's reagent, which produces very similar results, is a possible alternative but requires immersion at high temperature;
- the Murakami's reagent used to determine all the phases in one time.

As a result of accuracy analysis, a minimum number of image fields to obtain a precise phase quantification is 3. In Marble's reagent at least 6 images are required for precise evaluation of the phases.

However, it should be highlighted that the image analysis technique results in an error in the estimation of the phases present in the material. The phases can be overestimated or underestimated upon the etchant used. This fact, probably is related to both the resolution limit of optical microscopy and etching artifacts.

Future developments of this research may involve comparison with other reagents, e.g. using electrochemical etching techniques. This would better highlight the amount of deleterious phases studied in this paper with a low number of images. A useful approach, intermediate between light microscopy and XRD analysis, to determine the phase partition may be EBSD analysis with which to compare the results obtained in this research.

Author contribution statement

Francesco Sordetti: Conceptualization, Methodology, Validation, Formal analysis, Investigation, Writing – original draft; Alessandra Palombi: Formal analysis, Investigation, Writing – review & editing; Alessandra Varone: Validation, Resources, Writing – review & editing; Niki Picco: Investigation, Writing – review & editing; Michele Magnan: Investigation; Elia Marin: Writing – review & editing, Supervision; Claudio Maranzana: Resources; Alex Lanzutti: Resources, Writing – review & editing, Supervision.

Founding sources

This research did not receive any specific grant from funding agencies in the public, commercial, or not-for-profit sectors.

Declaration of competing interest

The authors declare that they have no known competing financial interests or personal relationships that could have appeared to influence the work reported in this paper.

Acknowledgements

The authors are grateful to Eng. Giovanni Beltrame (ZML Industries S. p.A., Viale dell'Industria 10, 33085 Maniago (PN), Italy) and Eng. Mirko Miorini (Pasello Trattamenti Termici S. r.l., Via della Torretta 39/a, 40012 Bargellino (BO), Italy) for their contribution to the analysis.

Appendix A

The integrated intensity of each peak can be written as [48]:

$$I = \frac{KRC}{2\mu}$$

where K is a constant, C the concentration of the phase (C = 1 for a single-phase material), μ the coefficient of linear absorption of the material while R is expressed by:

$$R = \left(\frac{1}{\nu^2}\right)\left[|F|^2 p\left(\frac{1+\cos^2 2\theta}{\sin^2\theta\cos\theta}\right)\right](e^{-2M})$$

being ν the volume of the unit cell, F the structure factor, p the factor of multiplicity, θ the Bragg angle, e^{-2M} the temperature factor and μ the coefficient of linear absorption of the material.

In the case of a material with different phases (e.g. α and β) and randomly oriented grains (e.g. powder), the ratio between the concentrations of α and β is proportional to the ratio between the intensities of one peak of α and one peak of β. In a bulk polycrystalline metal, where texture can be present, preferred orientations can influence relative intensity of the peaks. Therefore, the quantitative analysis must be carried out considering the integrated intensities of all the peaks [48].

In this case, three phases (ferrite α, austenite γ and σ phase) have been detected and the integrated intensities of each peak of α, γ and σ can be written as:

$$I_\gamma = \frac{KR_\gamma C_\gamma}{2\mu_m} \longrightarrow C_\gamma = \frac{2\mu_m I_\gamma}{KR_\gamma}$$

$$I_\alpha = \frac{K\ R_\alpha C_\alpha}{2\mu_m} \longrightarrow C_\alpha = \frac{2\mu_m I_\alpha}{KR_\alpha}$$

$$I_\sigma = \frac{KR_\sigma C_\sigma}{2\mu_m} \longrightarrow C_\sigma = \frac{2\mu_m I_\sigma}{KR_\sigma}$$

Being μ_m the average coefficient of linear absorption of the material consisting of three phases.

If a, b and c are the number of all XRD peaks of the phases α, γ and σ, respectively, the phase fractions can be expressed as:

$$C_\alpha = \frac{1}{a}\sum_1^a \frac{2\mu_m I_\alpha}{KR_\alpha}\ C_\gamma = \frac{1}{b}\sum_1^b \frac{2\mu_m I_\gamma}{KR_\gamma}\ C_\sigma = \frac{1}{c}\sum_1^c \frac{2\mu_m I_\sigma}{KR_\sigma}$$

The phase fractions can be calculated by combining the equation with the relationship Cα + Cγ + Cσ = 1.

References

[1] Chail G, Kangas P. Super and hyper duplex stainless steels: structures, properties and applications. In: Procedia structural integrity. Elsevier B.V.; 2016. p. 1755–62. https://doi.org/10.1016/j.prostr.2016.06.221.

[2] Boillot P, Peultier J. Use of stainless steels in the industry: recent and future developments. Procedia Eng 2014;83:309–21. https://doi.org/10.1016/J.PROENG.2014.09.015.

[3] Gunn RN. Duplex stainless steels microstructure, properties and applications. first ed. Cambridge, England: Woodhead Publishing; 1997. https://doi.org/10.1533/9781845698775.24.

[4] S T, Łabanowski J. Effect of microstructure on impact toughness of duplex and superduplex stainless steels. Journal of Achievements in Materials and Manufacturing Engineering 2009;36.

[5] Cojocaru EM, Raducanu D, Nocivin A, Cinca I, Vintila AN, Serban N, Angelescu ML, Cojocaru VD. Influence of aging treatment on microstructure and tensile properties of a hot deformed UNS S32750 super duplex stainless steel (SDSS) alloy. Metals 2020;10:353. https://doi.org/10.3390/met10030353.

[6] Charles J. Super duplex stainless steels-structure and properties. In: Conference of duplex stainless stee. France: Les Editions de Physique, Les Ulis Cedex; 1991. p. 3–48.

[7] Bhadeshia HKDH, Honeycombe SR. Stainless steel. Steels 2006:259–86. https://doi.org/10.1016/B978-075068084-4/50014-5.

[8] Kangas P, Chai G. Duplex stainless steels for oil & gas applications. In: 17th APCCC; 2016.

[9] Lanzutti A, Andreatta F, Magnan M, Gerolin A, Fedrizzi L. Unexpected failure of cast superduplex stainless steel exposed to high chlorides containing water: from failure analysis to corrosion mechanisms settlement. Eng Fail Anal 2022;136:106196. https://doi.org/10.1016/j.engfailanal.2022.106196.

[10] J. Weber, Materials for sea water pumps and related systems, SULZER Brothers Limited (n.d.) 1–11.

[11] Cojocaru EM, Raducanu D, Nocivin A, Cojocaru VD. Influence of ageing treatment temperature and duration on σ-phase precipitation and mechanical properties of UNS S32750 SDSS alloy. J Adv Res 2021;30:53–61. https://doi.org/10.1016/j.jare.2020.11.005.

[12] Mészáros I, Bögre B. Microstructural and magnetic investigations of duplex steel. IOP Conf Ser Mater Sci Eng 2018;426:012034. https://doi.org/10.1088/1757-899X/426/1/012034.
[13] Muthupandi V, Bala Srinivasan P, Seshadri SK, Sundaresan S. Effect of weld metal chemistry and heat input on the structure and properties of duplex stainless steel welds. Mater Sci Eng, A 2003;358:9–16. https://doi.org/10.1016/S0921-5093(03)00077-7.
[14] Totten GE. Steel heat treatment: metallurgy and technologies. Taylor & Francis; 2006. https://books.google.it/books?id=ORil4pedzjEC.
[15] Deng B, Jiang YM, Gao J, Li J. Effect of annealing treatment on microstructure evolution and the associated corrosion behavior of a super-duplex stainless steel. J Alloys Compd 2010;493:461–4. https://doi.org/10.1016/j.jallcom.2009.12.127.
[16] Nilsson JO, Wilson A. Influence of isothermal phase transformations on toughness and pitting corrosion of super duplex stainless steel SAF 2507. Mater Sci Technol 1993;9:545–54. https://doi.org/10.1179/mst.1993.9.7.545.
[17] Martins M, Casteletti LC. Heat treatment temperature influence on ASTM A890 GR 6A super duplex stainless steel microstructure. Mater Char 2005;55:225–33. https://doi.org/10.1016/j.matchar.2005.05.008.
[18] Pardal JM, Souto S, Tavares M, Da Penha M, Fonseca C, Adailson De Souza J, Menezes Vieira L, Ferreira Gomes De Abreu H. Deleterious phases precipitation on superduplex stainless steel UNS S32750: characterization by light optical and scanning electron microscopy. Mater Res 2010;13(3). https://doi.org/10.1590/S1516-14392010000300020.
[19] Bernhardsson S. Duplex stainless Steels'91. In: Chen TH, Weng KL, Yang YR, editors. The corrosion resistance of duplex stainless steels, the iron and steel institute of Japan. Chiba, Japan: Nippon Convenction Center; 1991. p. 185–210.
[20] Cojocaru EM, Raducanu D, Alturaihi SS, Nocivin A, Coman G, Cojocaru VD. Influence of isochronal treatments on microstructure and mechanical properties of solution treated UNS S32750 SDSS alloy specimens. J Mater Res Technol 2020;9:7870–9. https://doi.org/10.1016/j.jmrt.2020.05.056.
[21] Herbsleb G, Schwaab P. Precipitation of intermetallic compounds, nitrides and carbides in AF 22 duplex steel and their influence on corrosion behavior in acids. Mannesmann forschungsber. 1983. p. 26.
[22] Hättestrand M, Larsson P, Chai G, Nilsson J-O, Odqvist J. Study of decomposition of ferrite in a duplex stainless steel cold worked and aged at 450–500°C. Mater Sci Eng, A 2009;499:489–92. https://doi.org/10.1016/j.msea.2008.09.021.
[23] Unnikrishnan K, Mallik AK. Aging behaviour of a duplex stainless steel. Mater Sci Eng 1987;95:259–65. https://doi.org/10.1016/0025-5416(87)90517-9.
[24] Duprez L, De Cooman B, Akdut N. Microstructure evolution during isothermal annealing of a standard duplex stainless steel type 1.4462. Steel Res 2000;71:417–22. https://doi.org/10.1002/srin.200001338.
[25] Lee YH, Kim KT, Lee YD, Kim KY. Effects of W substitution on ς and χ phase precipitation and toughness in duplex stainless steels. Mater Sci Technol 1998;14:757–64. https://doi.org/10.1179/mst.1998.14.8.757.
[26] Michalska J, Sozańska M. Qualitative and quantitative analysis of σ and χ phases in 2205 duplex stainless steel. Mater Char 2006;56:355–62. https://doi.org/10.1016/j.matchar.2005.11.003.
[27] Chen TH, Weng KL, Yang JR. The effect of high-temperature exposure on the microstructural stability and toughness property in a 2205 duplex stainless steel. Mater Sci Eng 2002;338:259–70. https://doi.org/10.1016/S0921-5093(02)00093-X.
[28] Okafor ICI, Carlson ON. Equilibrium studies on a chi phase-strengthened ferritic alloy. Metall Trans A 1978;9:1651–7. https://doi.org/10.1007/BF02661948.
[29] Duprez L, De Cooman BC, Akdut N. Proceedings of the 6th world duplex conference and expo. In: A.I.M. - Associazione Italiana di Metallurgia; 2000. p. 355. Milan.
[30] Martins M. Caracterização microestrutural-mecânica e resistência à corrosão do aço inoxidável super duplex ASTM A890/A890M grau 6A. Universidade de São Paulo; 2006. https://doi.org/10.11606/T.88.2006.tde-25102007-152307.
[31] Atamert S, King JE. Sigma-phase formation and its prevention in duplex stainless steels. J Mater Sci Lett 1993;12:1144–7. https://doi.org/10.1007/BF00420548.
[32] Hosseini V, Karlsson L, Wessman S, Fuertes N. Effect of sigma phase morphology on the degradation of properties in a super duplex stainless steel. Materials 2018;11:933. https://doi.org/10.3390/ma11060933.
[33] ASTM International. ASTM E562-19e1: Standard Test Method for Determining Volume Fraction by Systematic Manual Point Count 2019.
[34] McEnerney JW. Experience Manufacturing Alloy 19D (UNS S32001) Seam Welded Lean Duplex Stainless Steel Tubing for Subsea Umbilical Applications 2001:245–64. https://www.scopus.com/inward/record.uri?eid=2-s2.0-85069703916&partnerID=40&md5=c362e3163c17ca74e411e4670f220ae4.
[35] Sicupira FL, Sandim MJR, Sandim HRZ, Santos DB, Renzetti RA. Quantification of retained austenite by X-ray diffraction and saturation magnetization in a supermartensitic stainless steel. Mater Char 2016;115:90–6. https://doi.org/10.1016/J.MATCHAR.2016.03.023.
[36] Fedorov A, Zhitenev A, Strekalovskaya D, Kur A. Quantitative description of the microstructure of duplex stainless steels using selective etching. In: The 1st international electronic conference on metallurgy and metals. Basel Switzerland: MDPI; 2021. p. 4. https://doi.org/10.3390/IEC2M-09387.
[37] Vander Voort G, Lucas GM, Manilova EP. Metallography and microstructures of stainless steels and maraging steels. ASM Handbook 2004;9:670–700.
[38] Llorca-Isern N, López-Luque H, López-Jiménez I, Biezma MV. Identification of sigma and chi phases in duplex stainless steels. Mater Char 2016;112:20–9. https://doi.org/10.1016/j.matchar.2015.12.004.
[39] Vander Voort GF, editor. Metallography and microstructures. ASM International; 2004. https://doi.org/10.31399/asm.hb.v09.9781627081771.
[40] Vander Voort GF. Color metallography. Micros Today 2005;13:22–7. https://doi.org/10.1017/S1551929500053943.
[41] Vander Voort GF, Manilova EP. Hints for imaging phases in steels. Adv Mater Process 2005;163:32–7.
[42] Kisasoz A, Karaaslan A, Bayrak Y. Effect of etching methods in metallographic studies of duplex stainless steel 2205. Met Sci Heat Treat 2017;58:704–6. https://doi.org/10.1007/s11041-017-0081-5.
[43] Varbai B, Pickle T, Májlinger K. Development and comparison of quantitative phase analysis for duplex stainless steel weld. Period Polytech - Mech Eng 2018;62. https://doi.org/10.3311/PPme.12234.
[44] Vicente A de A, D'silva PA, de Souza RL, dos Santos IL, de Aguiar RR, Botelho Junior AB. The use of duplex stainless steel filler metals to avoid hot cracking in GTAW welding of austenitic stainless steel AISI 316L. International Journal of Advanced Engineering Research and Science 2020;7:345–55. https://doi.org/10.22161/ijaers.76.43.
[45] JCPDS, International centre for diffraction data, 19073 (n.d.).
[46] ASTM International. ASTM E562-19e1: Standard Test Method for Determining Volume Fraction by Systematic Manual Point Count 2019.
[47] Olsson C-OA, Hättestrand M, Magnusson H, Shinde D, Thuvander M. Early precipitation stages of sigma phase in alloy 28 studied with scanning electron microscopy and atom probe tomography. ISIJ Int 2021;61:881–7. https://doi.org/10.2355/isijinternational.ISIJINT-2020-591.
[48] Cullity BD. Elements of X-ray diffraction. second ed. Reading, Massachussets: Addison Wesley Publishing Company INC.; 1977.